Published in final edited form as:
Ultrasound Med Biol. 2011 October ; 37(10): 1667–1676. doi:10.1016/j.ultrasmedbio.2011.06.017.

Dual-mode IVUS Transducer for Image-Guided Brain Therapy: Preliminary Experiments

Carl D. Herickhoff[*], **Christy M. Wilson**[†], **Gerald A. Grant**[†], **Gavin W. Britz**[†], **Edward D. Light**[*], **Mark L. Palmeri**[*], **Patrick D. Wolf**[*], and **Stephen W. Smith**[*]

[*]Department of Biomedical Engineering, Duke University, Durham, NC, USA

[†]Division of Neurosurgery, Duke University Medical Center, Durham, NC, USA

Abstract

In this study, we investigated the feasibility of using 3.5-Fr IVUS catheters for minimally-invasive, image-guided hyperthermia treatment of tumors in the brain. Feasibility was demonstrated by: 1) retro-fitting a commercial 3.5-Fr IVUS catheter with a 5 × 0.5 × 0.22 mm PZT-4 transducer for 9-MHz imaging, and 2) testing an identical transducer for therapy potential with 3.3-MHz continuous-wave excitation. The imaging transducer was compared to a 9-Fr, 9-MHz ICE catheter when visualizing the post-mortem ovine brain, and was also used to attempt vascular access to an in vivo porcine brain. A net average electrical power input of 700 mW was applied to the therapy transducer, producing a temperature rise of +13.5°C at a depth of 1.5 mm in live brain tumor tissue in the mouse model. These results suggest that it may be feasible to combine the imaging and therapeutic capabilities into a single device as a clinically-viable instrument.

Keywords

dual-mode catheter transducer; ultrasound hyperthermia; intravascular ultrasound

INTRODUCTION

The long-term goal of this research is the development of a minimally-invasive, endovascular approach to administering localized, image-guided, ultrasound-induced hyperthermia in the brain. This localized delivery of hyperthermia would provide targeted control of drug release from thermosensitive liposomes and opening the blood-brain barrier, which would enhance chemotherapeutic drug delivery to malignant brain tumors. In previous studies, we investigated the feasibility of dual-mode intracranial catheter transducers with two different approaches: first by using 14-Fr, phased-array prototype transducers for focused tissue heating and real-time 3D intracranial imaging, and second by modeling and measuring acoustic output for various 3.5-Fr intravascular ultrasound (IVUS) catheter transducer apertures (Herickhoff et al. 2009; Herickhoff et al. 2010). In this work,

Contact information for Corresponding Author: Carl Herickhoff, Duke University, Rm 136 Hudson Hall, Durham, NC 27708, Work phone: (919)660-5450, Cell phone: (507)304-0446, Fax: (919)684-4488, cdh14@duke.edu.

we investigate the merit of using a dual-frequency PZT-4 transducer by fabricating and testing in vivo imaging and tissue-heating prototypes.

The current treatment options for malignant central nervous system (CNS) tumors are inadequate, due to lack of efficacy, toxicity, and poor penetration of the blood-brain barrier (Fadul et al. 1988; Wrensch et al. 1993; Cabantog and Bernstein 1994; Schottenfeld and Fraumeni 1996; Wilkins and Rengachary 1996; Mareel 1998; Mikkelsen 1998; Sawaya et al. 1998; Bernstein et al. 2000; Kleihues et al. 2000; Prados 2000; Lesniak 2005; CBTRUS 2008; ACS 2009). New methods are being developed which show promise to improve brain tumor treatment by enhancing drug delivery and using noninvasive approaches. The many examples of this would include: using localized hyperthermia and targeted, thermosensitive liposomes (drug release threshold +4°C above body temperature); opening the blood-brain barrier using ultrasound, with or without microbubble contrast agent; and transcranial, image-guided focused ultrasound for thermal ablation (Guthkelch et al. 1991; Zunkeler et al. 1996; Hynynen and Jolesz 1998; Kroll and Neuwelt 1998; Hynynen et al. 2001; Cho et al. 2002; Dayton and Ferrara 2002; Mesiwala et al. 2002; Aubry et al. 2003; Bloch et al. 2004; Hynynen et al. 2004; Ponce et al. 2006; Choi et al. 2007; Kheirolomoom et al. 2007; McDannold et al. 2007; McDannold et al. 2008; Vykhodtseva et al. 2008; McDannold et al. 2010).

Dual-mode ultrasound devices for image-guided therapy have been designed and implemented for many different applications using various approaches (Hynynen 1997; Wu et al. 2001; Barthe et al. 2004; Gentry and Smith 2004; Makin et al. 2005; Ebbini et al. 2006; Pua et al. 2007; Bouchoux et al. 2008; Bouchoux et al. 2010). Intravascular ultrasound (IVUS) catheters, which are typically less than 4 Fr, were developed to navigate into coronary vessels to visualize and characterize atherosclerotic plaque (Fishbein and Siegel 1998; Mehran et al. 1998; Nishioka et al. 1998; Uren et al. 1998a; Uren et al. 1998b). Mechanical IVUS catheters commonly use a single rotating piezoelectric crystal with a surface area less than a few square millimeters, and the use of IVUS catheters for therapeutic applications involving microbubbles is being investigated (Foster et al. 1993; Erbel 1998; Phillips et al. 2008; Kilroy et al. 2009). Furthermore, interventional neuroradiologists have used minimally-invasive endovascular techniques to treat intracranial diseases, including inserting a 5-Fr catheter as far as the frontal portion of the superior sagittal sinus to treat thrombosis, and these procedures can be extended to the treatment of intracranial tumors (Horowitz et al. 1995; Kuether et al. 1998; Connors and Wojak 1999; Dowd et al. 1999; Opatowsky et al. 1999; Chow et al. 2000; Novak et al. 2000; Morris 2002).

Our design goal is a dual-mode ultrasound catheter that is both thin and flexible enough to navigate a vascular pathway to the brain and be placed immediately adjacent to a brain tumor target, to visualize the tumor and then direct an ultrasound hyperthermia beam to trigger the release of drugs contained within thermosensitive liposomes molecularly targeted to regions of tumor angiogenesis (see Figure 1). Commercially-available IVUS catheters have an appropriate form factor—are both thin and flexible enough—to achieve the desired placement within the brain volume via our intended vascular approach, so they are considered here as one possible platform for a dual-mode intracranial catheter integrating ultrasound imaging and hyperthermia.

In this paper, we describe the construction and testing of two prototypes (one for imaging, the other for therapy), each using an identical, dual-frequency PZT-4 transducer element, to independently assess imaging performance and therapeutic potential of the proposed dual-mode, intracranial IVUS catheter design.

MATERIALS & METHODS

For our prototypes, PZT-4 was used because its properties (high k_T and Q_m, low tan δ) make it an excellent choice of material for dual-mode imaging and therapy transducers. A 9-MHz resonance for imaging corresponds to a PZT-4 thickness of 0.22 mm, and the maximum-allowable aperture geometry for a flexible 3.5-Fr IVUS catheter was determined to be 5 × 0.5 mm in consultation with neurosurgery and interventional neuroradiology colleagues. In addition to the thickness-mode, a width-mode resonance at 3.3 MHz was designed and utilized for increased thermal penetration depth. Consequently, two prototypes were built using 5 × 0.5 × 0.22 mm PZT-4: one to assess imaging performance at 9 MHz in a mechanical IVUS catheter, and one to assess therapeutic potential by hyperthermia generation at 3.3 MHz.

Imaging

For the imaging prototype, a mechanical IVUS catheter was needed as a construction template. A Boston Scientific (Natick, MA, USA) Atlantis™ SR Pro coronary imaging catheter, with a nominal frequency of 40 MHz, was chosen and tested prior to modification by connecting to a ClearView Ultra™ scanner. Figure 2 shows a 40-MHz image of a portion of a 2.5-cm-diameter cyst phantom acquired with the unmodified Atlantis.

The Atlantis' original 40-MHz element was carefully removed from the distal end of the catheter, and the rounded metal housing was filed down to create a level shelf. The 5 × 0.5 × 0.22 mm PZT-4 element was then bonded to the shelf with silver epoxy (CHO-BOND, Chomerics, Woburn, MA, USA) to secure and electrically connect to the ground contact on the back of the element. The front contact was then connected to the signal wire—protruding from the middle of the housing—with silver epoxy. To reinforce the delicate bonds of silver epoxy, a coating of 20-minute epoxy (Finish-Cure, Bob Smith Industries, Atascadero, CA, USA) was applied around the proximal end of the element. Finally, to ensure that sound was transmitted and received only through the front face of the transducer, an improvised air backing was created using a mixture of 20-minute epoxy and phenolic microballoons (BJO-0930, Asia Pacific Microballoons, Selangor, Malaysia). Figure 3 shows a top-view and side-view schematic of the prototype.

To initially assess imaging performance, the modified Atlantis IVUS prototype was compared to a Boston Scientific 9-Fr intracardiac echo catheter (Ultra ICE™; see Figure 4a) as a gold standard for 9-MHz imaging. Using the ClearView Ultra scanner, each catheter was used to image two targets: a 2.5-cm-diameter cyst phantom, and three post-mortem ovine brains. To image the ovine brain 30 minutes post-mortem, a burr hole was made along the midline of the skull, angled posteriorly. This allowed catheter insertion into the superior sagittal sinus, such that the imaging plane (perpendicular to the catheter axis) could be swept over the brain volume by push-through or pull-back (see Figure 5).

The final experiment with the 9-MHz imaging prototype attempted to access the cranial cavity via a minimally-invasive vascular approach in an in vivo porcine model. The Institutional Animal Care and Use Committee at Duke University approved the following procedure. An intravenous (IV) line was established in a peripheral vein and the animal was sedated with thiopental sodium, 20 mg/kg administered intravenously. Anesthesia was induced with inhalation of isoflurane gas 1% to 5 % delivered through a nose cone. The animal was intubated, placed on a water heated thermal pad, and started on a ventilator. A line was placed in the left femoral artery via a percutaneous puncture or cutdown. Electrolyte and ventilator adjustments were made based on serial electrolyte and arterial blood gas measurements. An IV maintenance drip of D-5 lactated Ringer's solution was started and maintained at 5 mL/kg/min. Blood pressure, lead II electrocardiogram, and

temperature were continuously monitored throughout the procedure. The animal was placed in a supine position, and the right femoral artery was punctured using the Seldinger technique and dilated over a guide wire. A preliminary angiogram of the right common carotid and vertebral arteries was performed and recorded to identify the locations and anatomy of proximate branch vessels. With a 6-Fr Envoy™ XB (670-258-90B, Cordis Corp., Bridgewater, NJ, USA) guiding catheter in place over a wire guide, the modified Atlantis IVUS prototype was advanced toward the cranial vessels via either the carotid or vertebral arteries. Real-time images of the vessels and surrounding tissue were acquired at 9 MHz using the ClearView Ultra scanner.

Therapy

A therapy prototype designed for high-power operation was constructed using a piece of PZT-4 identical to that used in the 9-MHz imaging prototype (5 × 0.5 × 0.22 mm). Double-sided metallized liquid crystal polymer (LCP, 20 μm thick) was bonded to the face of the ceramic with silver epoxy, to provide both a signal ground contact and a separate outer ground layer to shield RF noise. Four feet of IVUS-catheter coaxial cable was removed from the inside of a spare Atlantis catheter, and the cable's ground and signal wires were carefully exposed and separated at the distal end before being bonded to the front and back contacts of the PZT-4, respectively. An epoxy-and-microballoons air backing was applied (similar to the imaging prototype), and the transducer was secured and sealed in a 9-Fr catheter scrap, in side-viewing configuration.

An impedance analyzer (Model 4194A, Hewlett-Packard, Palo Alto, CA, USA) was used to measure the electrical impedances of both the therapy prototype and a 25-W RF power amplifier (Model 525LA, ENI, Rochester, NY, USA) at 3.3 MHz. These impedance values were used to calculate the optimal inductance and capacitance values (7.7 μH and 55 pF, respectively) for the design of a simple L-section impedance matching network, which would be used to maximize power transfer from the power source (amplifier) to the load (therapy prototype transducer) at a single frequency (3.3 MHz).

To initially assess therapeutic potential, the transducer was used in vitro with tissue-mimicking material (National Physical Laboratory, Teddington, UK), which is 4 cm in diameter and 4 mm thick, and has thermal properties similar to brain tissue (Goss et al. 1978; Bacon and Shaw 1993; Shaw et al. 1999). To measure the achievable temperature, a type T, 33-gauge, hypodermic needle thermocouple (HYP-0, Omega Engineering, Stamford, CT, USA) was used. This small-diameter, fine-wire thermocouple sheathed in stainless steel was chosen to minimize the possibility of artifacts (e.g. viscous heating, reflections, conduction along the wire) in the thermal measurement (Fry and Fry 1954; Hynynen and Edwards 1989). We do not otherwise consider these effects in the proof-of-concept experiments described here.

The thermocouple was inserted approximately 1 mm beneath the surface of the material, and the depth of the thermocouple was verified by imaging the sample with a Vevo 770™ scanner and RMV706™ scanhead (VisualSonics, Toronto, Ontario, Canada) at 40 MHz (see Figure 6a). The prototype transducer was aligned with the thermocouple and placed within 1 mm of the surface of the submerged material sample (see Figure 6b). A waveform generator (Model 33250, Agilent, Santa Clara, CA, USA) was connected to the power amplifier to produce continuous-wave (CW) excitation at a net average electric power of 700 mW at 3.3 MHz for nearly 2 minutes while the thermocouple recorded temperature. Electrical input to the matching network and therapy prototype transducer, including average forward and reflected power, was measured using a power reflection meter (NRT, Rohde & Schwarz, Munich, Germany).

The therapy prototype transducer was tested on an excised glioblastoma tumor, which had been grown artificially on the flank of a nude mouse. The tumor measured 13 mm along the long axis, and 10 mm along the short axis. A minimal amount of standard ultrasound transmission gel (Conductor, Chattanooga Group, Hixson, TN, USA) was applied to the face of the transducer before placing it in contact with the tumor. The thermocouple was inserted approximately 1.5 mm beneath the surface of the tissue, and aligned with the center of the transducer. The waveform generator and power amplifier created 3.3 MHz CW excitation. The power was alternately turned on and off for 90 seconds at a time, at levels of 700, 350, and 175 mW, while the thermocouple recorded temperature.

Finally, the therapy prototype was tested on a human glioblastoma xenograft tumor, grown to approximately 1 cm × 2 cm in the flank of a nude mouse. The animal was anesthetized with 100mg/kg ketamine/xylazine and monitored by toe pinch reflex. The anesthetic was re-administered as needed on a per animal basis, when the animal responded to the toe-pinch. Animal body temperature was maintained at 37°C using a homeothermic heating blanket. The skin around the tumor was carefully dissected away so that the transducer could be placed directly on the surface of the tumor, using minimal ultrasound transmission gel. The tumor measured 18 mm along the long axis, and 16 mm along the short axis. The thermocouple was inserted approximately 1.5 mm beneath the tissue surface and aligned with the transducer (see Figure 6c). The waveform generator and power amplifier produced 3.3-MHz CW excitation for 60 seconds, followed by 120 seconds of off-time, to allow the tissue temperature to recover to nearer its baseline temperature. This was done sequentially at power levels of 700, 350, and 175 mW, while the thermocouple recorded temperature.

RESULTS

Imaging

Figure 4a shows the 9-Fr ICE catheter used as an imaging gold standard, and the modified Atlantis IVUS prototype transducer is shown in Figure 4c. The ICE transducer is 2.1 mm in diameter, while the IVUS prototype has an aperture 0.5 mm in azimuth. Figures 4b and 4d are 9-MHz images of a 2.5-cm cyst phantom acquired by the commercial 9-Fr ICE catheter and the 3.5-Fr modified IVUS prototype, respectively. Though the gold-standard ICE catheter outperforms the prototype in terms of lateral resolution and sensitivity, the images are roughly comparable. The IVUS prototype has greater degree of beam divergence due to its much smaller aperture, resulting in poorer lateral resolution relative to the ICE gold standard.

Figure 7 compares the imaging performance of the 9-Fr ICE and 3.5-Fr modified IVUS catheter probes in a post-mortem ovine brain, with an anatomical diagram for reference. In both images, the skull is seen outlining the cranial cavity, and the symmetric wings of the lateral ventricles are clearly visible in the center of the brain volume as well.

In the in vivo porcine experiment, the prototype catheter was unfortunately unable to advance beyond the pig’s vertebral artery into the basilar artery at the base of the brain. Figure 8 shows the prototype transducer at its farthest advancement in the vertebral artery, as well as a real-time, 9-MHz ultrasound image of the vertebral artery near the subclavian junction.

Therapy

In the tissue-mimicking material, the 3.3-MHz therapy prototype transducer was able to create a temperature rise of 6.7°C in less than 2 m inutes with CW transmission at 700 mW (see Figure 9). In the excised glioblastoma brain tumor, the therapy prototype created a temperature rise of 19.1°C in 90 seconds of CW excitation at 70 0 mW. Subsequently,

temperature rises of 9.2°C and 4.9°C were created using 350 mW and 175 m W of CW power, respectively (see Figure 10). Finally, in the in vivo tumor experiment, the therapy prototype achieved temperature rises of 13.5°C, 6.8°C, and 3.0°C in 60 seconds of CW excitation at 700, 350, and 175 mW, respectively (see Figure 11).

DISCUSSION

A 5 × 0.5 × 0.22 mm PZT-4 transducer was used to build a 9-MHz imaging prototype in a 3.5-Fr mechanical IVUS catheter, and a 3.3-MHz high-power prototype for therapy. The 3.5-Fr imaging prototype performed comparably to a 9-Fr commercial ICE catheter in imaging a 2.5-cm cyst phantom and visualizing brain anatomy in a post-mortem ovine brain. The ovine brain images show that a 3.5-Fr IVUS catheter is capable of resolving features (including the lateral ventricles and skull) at a depth of up to 3 cm.

To our knowledge, we have shown the first attempt to access and image the brain via a minimally-invasive, vascular approach using an ultrasound catheter. The 3.5-Fr, 9-MHz modified-Atlantis imaging prototype was able to navigate as far as the vertebral artery and image surrounding tissue before vessel narrowing and tortuosity prevented further catheter advancement. Although access to the brain volume was not achieved in the porcine model, the authors' experience in the field of interventional neuroradiology gives confidence that such restricting vessel size and tortuosity issues would not be present in a human procedure.

The results from the 3.5-Fr, 9-MHz IVUS imaging prototype can be compared to the findings of two final experiments using a 20-MHz Volcano (San Diego, CA, USA) 3.5-Fr phased-array IVUS imaging catheter with an In-Vision™ scanner. First, a Volcano Eagle Eye™ Gold was used in the same porcine model experiment as the modified Atlantis, to visualize the vessel and its surroundings with a higher-frequency, commercial IVUS catheter. As the Eagle Eye was advanced into the vertebral artery, the wire guide accidentally punctured the vessel wall, creating a regional hematoma which was visible under fluoroscopy (see Figure 12a). The turbulent blood flow created by the puncture was visible when using the scanner's ChromaFlo ™ feature to image the lumen (see Figure 12b).

The other auxiliary experiment used a Volcano PV018 catheter to visualize structures near the brain surface. The 3.5-Fr catheter was inserted through a 1-cm burr hole in a porcine skull, placing the IVUS array between the inner surface of the skull and the dura mater, a few millimeters adjacent to the midline. The scan depth was maximized to 12 mm, and features including cerebral gyri, sulci, and pulsating vessels could be clearly seen out to a range of 5-6 mm (see Figure 13). The findings from these auxiliary experiments suggest that additional useful information might be obtained with a more sophisticated device designed to operate at a frequency above 9 MHz.

The therapy prototype achieved a temperature rise of 6.7°C in tissue-mimicking material before testing tissue-heating capability in glioblastoma tumors. In an excised tumor, the therapy prototype achieved a temperature rise as high as 19.1°C in 90 seconds at 1.5 mm deep. When similarly tested on an in vivo tumor, the prototype achieved a temperature rise of 13.5°C in 60 seconds.

The sharp rise and fall of the temperature data as power was turned on and off in the tumor therapy experiments (Figures 10 & 11) further suggests that the observed heating was predominantly due to absorption of ultrasound energy (not conduction), and it also demonstrates the range and control of achievable tissue temperatures using an IVUS-sized transducer (Frinkley et al. 2005). The sequential excitations were effectively set at 100% power, 50% power, and 25% power, and the resulting increases in temperature were proportional.

The lower temperature increase in the tissue-mimicking material, relative to the tumor experiment results, is likely due to the fact that the transducer was not directly in contact with the tissue. This may have allowed for some amount of divergence and reflection of the ultrasound energy beam (Herickhoff et al. 2010). The presence of a water path also served to somewhat isolate the sample from any conductive heating contributions that may have been present. The 19.1°C and 13.5°C increases in the ex cised and in vivo tumor experiments were much higher than the minimum increase of 4°C necess ary for drug release from thermosensitive liposomes, demonstrating that it is possible to facilitate thermally-targeted drug delivery using a transducer small enough to be packaged in a 3.5-Fr IVUS catheter. The challenges that remain for realizing a dual-mode, image-guided therapy catheter device include further improving efficiency (by incorporating acoustic matching layers), packaging, and wiring to electronics capable of both higher-frequency pulsed excitation (for imaging) and lower-frequency continuous-wave excitation (for therapy).

CONCLUSIONS

In total, the images obtained using the 3.5-Fr modified Atlantis prototype and commercially-available Volcano catheters in brain and vascular-access experiments demonstrate that it is possible to use an intravascular ultrasound device to effectively visualize structures in the brain which are in close proximity to the transducer, and that catheter probes may be placed intracranially via a minimally-invasive vascular approach. It was also shown that a 5 × 0.5 × 0.22 mm PZT-4 transducer is capable of heating a tumor in vivo +13.5°C above baseline temperature, a value well above the +4°C threshold for drug release from thermosensitive liposomes.

Our results indicate that combining these imaging and therapeutic capabilities into a single dual-mode device may be feasible, and this could yield a clinically-viable technology for brain tumor treatment. Future experiments will investigate the therapeutic effect such a device may have on an intracranial brain tumor.

Acknowledgments

The authors thank Volcano Corporation for their support in this study, as well as Veronica Rotemberg, Samantha Lipman, Josh Doherty, Tat-Jin Teo, Rick Stouffer, and Ellen Dixon-Tulloch for their assistance. This work was supported by NIH grant HL089507.

References

ACS. Cancer Facts & Figures 2009. Atlanta: American Cancer Society; 2009. p. 4

Aubry JF, Tanter M, Pernot M, Thomas JL, Fink M. Experimental demonstration of noninvasive transskull adaptive focusing based on prior computed tomography scans. J Acoust Soc Am. 2003; 113:84–93. [PubMed: 12558249]

Bacon DR, Shaw A. Experimental Validation of Predicted Temperature Rises in Tissue-Mimicking Materials. Physics in Medicine and Biology. 1993; 38:1647–59. [PubMed: 8272439]

Barthe, PG.; Slayton, MH.; Jaeger, PM.; Makin, IRS.; Gallagher, LA.; Mast, TD.; Runk, MM.; Faidi, W. Ultrasound Therapy System and Ablation Results Utilizing Miniature Imaging/Therapy Arrays. 2004 IEEE Ultrasonics Symposium; Montreal. 2004. p. 1792-5.

Bernstein, M.; Berger, MS. American Association of Neurological Surgeons. Joint Tumor Section., Congress of Neurological Surgeons. Neuro-oncology : the essentials. New York: Thieme Medical Publishers; 2000.

Bloch SH, Dayton PA, Ferrara KW. Targeted imaging using ultrasound contrast agents. IEEE Eng Med Biol Mag. 2004; 23:18–29. [PubMed: 15565796]

Bouchoux G, Lafon C, Berriet R, Chapelon JY, Fleury G, Cathignol D. Dual-mode ultrasound transducer for image-guided interstitial thermal therapy. Ultrasound in Medicine and Biology. 2008; 34:607–16. [PubMed: 18055099]

Bouchoux G, Owen NR, Chavrier F, Berriet R, Fleury G, Chapelon JY, Lafon C. Interstitial Thermal Ablation With a Fast Rotating Dual-Mode Transducer. Ieee Transactions on Ultrasonics Ferroelectrics and Frequency Control. 2010; 57:1086–95.

Cabantog AM, Bernstein M. Complications of First Craniotomy for Intraaxial Brain-Tumor. Canadian Journal of Neurological Sciences. 1994; 21:213–8. [PubMed: 8000976]

CBTRUS. Statistical Report: Primary Brain Tumors in the United States, 2000-2004. Vol. 10. Central Brain Tumor Registry of the United States; 2008. p. 7-8.

Cho CW, Liu Y, Cobb WN, Henthorn TK, Lillehei K, Christians U, Ng KY. Ultrasound-induced mild hyperthermia as a novel approach to increase drug uptake in brain microvessel endothelial cells. Pharmaceutical Research. 2002; 19:1123–9. [PubMed: 12240937]

Choi JJ, Pernot M, Small SA, Konofagou EE. Noninvasive, transcranial and localized opening of the blood-brain barrier using focused ultrasound in mice. Ultrasound in Medicine and Biology. 2007; 33:95–104. [PubMed: 17189051]

Chow K, Gobin YP, Saver J, Kidwell C, Dong P, Vinuela F. Endovascular treatment of dural sinus thrombosis with rheolytic thrombectomy and intra-arterial thrombolysis. Stroke. 2000; 31:1420–5. [PubMed: 10835466]

Connors, JJ.; Wojak, JC. Interventional neuroradiology : strategies and practical techniques. Philadelphia: Saunders; 1999.

Dayton PA, Ferrara KW. Targeted imaging using ultrasound. Journal of Magnetic Resonance Imaging. 2002; 16:362–77. [PubMed: 12353252]

Dowd CF, Malek AM, Phatouros CC, Hemphill JC. Application of a rheolytic thrombectomy device in the treatment of dural sinus thrombosis: A new technique. American Journal of Neuroradiology. 1999; 20:568–70. [PubMed: 10319961]

Ebbini ES, Yao H, Shrestha A. Dual-mode ultrasound phased arrays for image-guided surgery. Ultrasonic Imaging. 2006; 28:65–82. [PubMed: 17094688]

Erbel, R. Intravascular ultrasound. St. Louis: Mosby; 1998.

Fadul C, Wood J, Thaler H, Galicich J, Patterson RH, Posner JB. Morbidity and Mortality of Craniotomy for Excision of Supratentorial Gliomas. Neurology. 1988; 38:1374–9. [PubMed: 3412585]

Fishbein, MC.; Siegel, RJ. Pathology of coronary atherosclerosis: implications for intravascular ultrasound imaging. In: Siegel, RJ., editor. Intravascular ultrasound imaging in coronary artery disease. New York: Dekker; 1998. p. 1-17.

Fletcher TF, Hardy RM, Feeney DA. Canine Planar Anatomy. 2006 Online.

Foster, FS.; Ryan, LK.; Lockwood, GR. High frequency ultrasound scanning of the arterial wall. In: Roelandt, J., editor. Intravascular ultrasound. Dordrecht ; Boston: Kluwer Academic Publishers; 1993. p. 91-108.

Frinkley K, Palmeri M, Nightingale K. Controlled spatio-temporal heating patterns using a commercial, diagnostic ultrasound system. 2005 IEEE Ultrasonics Symposium. 2005; 1-4:1130–4.

Fry WJ, Fry RB. Determination of Absolute Sound Levels and Acoustic Absorption Coefficients by Thermocouple Probes - Experiment. Journal of the Acoustical Society of America. 1954; 26:311–7.

Gentry KL, Smith SW. Integrated catheter for 3-D intracardiac echo cardiography and ultrasound ablation. Ieee Transactions on Ultrasonics Ferroelectrics and Frequency Control. 2004; 51:800–8.

Goss SA, Johnston RL, Dunn F. Comprehensive Compilation of Empirical Ultrasonic Properties of Mammalian-Tissues. Journal of the Acoustical Society of America. 1978; 64:423–57. [PubMed: 361793]

Guthkelch AN, Carter LP, Cassady JR, Hynynen KH, Iacono RP, Johnson PC, Obbens EAMT, Roemer RB, Seeger JF, Shimm DS, Stea B. Treatment of Malignant Brain-Tumors with Focused Ultrasound Hyperthermia and Radiation - Results of a Phase-I Trial. Journal of Neuro-Oncology. 1991; 10:271–84. [PubMed: 1654406]

Herickhoff CD, Grant GA, Britz GW, Smith SW. Dual-Mode IVUS Catheter for Intracranial Image-Guided Hyperthermia: Feasibility Study. Ieee Transactions on Ultrasonics Ferroelectrics and Frequency Control. 2010; 57:2572–84.

Herickhoff CD, Light ED, Bing KF, Mukundan S, Grant GA, Wolf PD, Smith SW. Dual-Mode Intracranial Catheter Integrating 3D Ultrasound Imaging and Hyperthermia for Neuro-oncology: Feasibility Study. Ultrasonic Imaging. 2009; 31:81–100. [PubMed: 19630251]

Horowitz M, Purdy P, Unwin H, Carstens G, Greenlee R, Hise J, Kopitnik T, Batjer H, Rollins N, Samson D. Treatment of Dural Sinus Thrombosis Using Selective Catheterization and Urokinase. Annals of Neurology. 1995; 38:58–67. [PubMed: 7611726]

Hynynen, K. Review of Ultrasound Therapy. 1997 IEEE Ultrasonics Symposium; Toronto. 1997. p. 1305-13.

Hynynen K, Clement GT, McDannold N, Vykhodtseva N, King R, White PJ, Vitek S, Jolesz FA. 500-element ultrasound phased array system for noninvasive focal surgery of the brain: a preliminary rabbit study with ex vivo human skulls. Magn Reson Med. 2004; 52:100–7. [PubMed: 15236372]

Hynynen K, Edwards DK. Temperature-Measurements during Ultrasound Hyperthermia. Medical Physics. 1989; 16:618–26. [PubMed: 2549354]

Hynynen K, Jolesz FA. Demonstration of potential noninvasive ultrasound brain therapy through an intact skull. Ultrasound in Medicine and Biology. 1998; 24:275–83. [PubMed: 9550186]

Hynynen K, McDannold N, Vykhodtseva N, Jolesz FA. Noninvasive MR imaging-guided focal opening of the blood-brain barrier in rabbits. Radiology. 2001; 220:640–6. [PubMed: 11526261]

Kheirolomoom A, Dayton PA, Lum AFH, Little E, Paoli EE, Zheng HR, Ferrara KW. Acoustically-active microbubbles conjugated to liposomes: Characterization of a proposed drug delivery vehicle. Journal of Controlled Release. 2007; 118:275–84. [PubMed: 17300849]

Kilroy, JP.; Patil, AV.; Hossack, JA. Ultrasound Catheter for Microbubble Based Drug Delivery. IEEE Ultrasonics Symp; Rome. 2009. p. 2770-3.

Kleihues, P.; Cavenee, WK. International Agency for Research on Cancer., International Society of Neuropathology., International Academy of Pathology., Preuss Foundation for Brain Tumor Research. Pathology and genetics of tumours of the nervous system. Lyon: IARC Press; 2000.

Kroll RA, Neuwelt EA. Outwitting the blood-brain barrier for therapeutic purposes: Osmotic opening and other means. Neurosurgery. 1998; 42:1083–99. [PubMed: 9588554]

Kuether TA, O'Neill O, Nesbit GM, Barnwell SL. Endovascular treatment of traumatic dural sinus thrombosis: Case report. Neurosurgery. 1998; 42:1163–6. [PubMed: 9588564]

Lesniak, MS. Targeting Drugs to Tumors of the Central Nervous System. In: Ali-Osman, F., editor. Brain Tumors. Totowa, N.J.: Humana Press; 2005. p. 353

Makin IRS, Mast TD, Faidi W, Runk MM, Barthe PG, Slayton MH. Miniaturized ultrasound arrays for interstitial ablation and imaging. Ultrasound in Medicine and Biology. 2005; 31:1539–50. [PubMed: 16286031]

Mareel, M. Anti-Invasive Brain Tumor Therapy: General Aspects and Future Strategies. In: Mikkelsen, T., editor. Brain Tumor Invasion: Biological, Clinical, and Therapeutic Considerations. New York: Wiley-Liss; 1998. p. 391-414.

McDannold N, Clement GT, Black P, Jolesz F, Hynynen K. Transcranial Magnetic Resonance Imaging-Guided Focused Ultrasound Surgery of Brain Tumors: Initial Findings in 3 Patients. Neurosurgery. 2010; 66:323–32. [PubMed: 20087132]

McDannold N, Vykhodtseva N, Hynynen K. Use of ultrasound pulses combined with Definity for targeted blood-brain barrier disruption: a feasibility study. Ultrasound Med Biol. 2007; 33:584–90. [PubMed: 17337109]

McDannold N, Vykhodtseva N, Hynynen K. Blood-brain barrier disruption induced by focused ultrasound and circulating preformed microbubbles appears to be characterized by the mechanical index. Ultrasound Med Biol. 2008; 34:834–40. [PubMed: 18207311]

Mehran, R.; Mintz, GS.; Pichard, AD.; Kent, KM.; Satler, LF.; Popma, JJ.; Leon, MB. Clinical application of intravascular ultrasound imaging in a center with high-volume preintervention ultrasound imaging. In: Siegel, RJ., editor. Intravascular ultrasound imaging in coronary artery disease. New York: Dekker; 1998. p. 59-73.

Mesiwala AH, Farrell L, Wenzel HJ, Silbergeld DL, Crum LA, Winn HR, Mourad PD. High-intensity focused ultrasound selectively disrupts the blood-brain barrier in vivo. Ultrasound in Medicine and Biology. 2002; 28:389–400. [PubMed: 11978420]

Mikkelsen, T. Brain tumor invasion : biological, clinical, and therapeutic considerations. New York: Wiley-Liss; 1998.

Miselis RR. Neuroscience Laboratory : Laboratory 2-3 : Gross Brain and Spinal Cord. 2006 Online.

Morris, P. Interventional and endovascular therapy of the nervous system : a practice guide. New York: Springer; 2002.

Nishioka, T.; Luo, H.; Eigler, NL.; Siegel, RJ.; Tabak, SW. Clinical application of IVUS imaging in a center with selective use of IVUS imaging. In: Siegel, RJ., editor. Intravascular ultrasound imaging in coronary artery disease. New York: Dekker; 1998. p. 75-94.

Novak Z, Coldwell DM, Brega KE. Selective infusion of urokinase and thrombectomy in the treatment of acute cerebral sinus thrombosis. American Journal of Neuroradiology. 2000; 21:143–5. [PubMed: 10669240]

Opatowsky MJ, Morris PP, Regan JD, Mewborne JD, Wilson JA. Rapid thrombectomy of superior sagittal sinus and transverse sinus thrombosis with a rheolytic catheter device. American Journal of Neuroradiology. 1999; 20:414–7. [PubMed: 10219406]

Phillips, LC.; Klibanov, AL.; Wamhoff, BR.; Hossack, JA. Intravascular Ultrasound Mediated Delivery of DNA via Microbubble Carriers to an Injured Porcine Artery *In Vivo*. IEEE Ultrasonics Symp; Beijing. 2008. p. 1154-7.

Ponce AM, Vujaskovic Z, Yuan F, Needham D, Dewhirst MW. Hyperthermia mediated liposomal drug delivery. International Journal of Hyperthermia. 2006; 22:205–13. [PubMed: 16754340]

Prados, MD. Systemic Chemotherapy. In: Bernstein, M.; Berger, MS., editors. Neuro-oncology: The Essentials. New York: Thieme Medical Publishers; 2000. p. 228-9.

Pua EC, Qiu YP, Smith SW. Integrated endoscope for real-time 3D ultrasound imaging and hyperthermia: Feasibility study. Ultrasonic Imaging. 2007; 29:1–14. [PubMed: 17491295]

Sawaya R, Hammoud M, Schoppa D, Hess KR, Wu SZ, Shi WM, Wildrick DM. Neurosurgical outcomes in a modern series of 400 craniotomies for treatment of parenchymal tumors. Neurosurgery. 1998; 42:1044–55. [PubMed: 9588549]

Schottenfeld, D.; Fraumeni, JF. Cancer epidemiology and prevention. New York: Oxford University Press; 1996.

Shaw A, Pay NM, Preston RC, Bond AD. Proposed standard thermal test object for medical ultrasound. Ultrasound in Medicine and Biology. 1999; 25:121–32. [PubMed: 10048809]

Uren, NG.; Yock, PG.; Fitzgerald, PJ. Intravascular ultrasound image interpretation: normal arteries, abnormal vessels, and atheroma types pre- and postintervention. In: Siegel, RJ., editor. Intravascular ultrasound imaging in coronary artery disease. New York: Dekker; 1998a. p. 19-37.

Uren, NG.; Yock, PG.; Fitzgerald, PJ. Prognostic implications of intravascular ultrasound imaging after coronary intervention. In: Siegel, RJ., editor. Intravascular ultrasound imaging in coronary artery disease. New York: Dekker; 1998b. p. 39-57.

Vykhodtseva N, McDannold N, Hynynen K. Progress and problems in the application of focused ultrasound for blood-brain barrier disruption. Ultrasonics. 2008; 48:279–96. [PubMed: 18511095]

Welker WI. Comparative Mammalian Brain Collections. 2011 Online.

Wilkins, RH.; Rengachary, SS. Neurosurgery. New York: McGraw-Hill, Health Professions Division; 1996.

Wrensch M, Bondy ML, Wiencke J, Yost M. Environmental Risk-Factors for Primary Malignant Brain-Tumors - a Review. Journal of Neuro-Oncology. 1993; 17:47–64. [PubMed: 8120572]

Wu F, Chen WZ, Bai J, Zou JZ, Wang ZL, Zhu H, Wang ZB. Pathological changes in human malignant carcinoma treated with high-intensity focused ultrasound. Ultrasound in Medicine and Biology. 2001; 27:1099–106. [PubMed: 11527596]

Zunkeler B, Carson RE, Olson J, Blasberg RG, DeVroom H, Lutz RJ, Saris SC, Wright DC, Kammerer W, Patronas NJ, Dedrick RL, Herscovitch P, Oldfield EH. Quantification and pharmacokinetics of blood-brain barrier disruption in humans. Journal of Neurosurgery. 1996; 85:1056–65. [PubMed: 8929495]

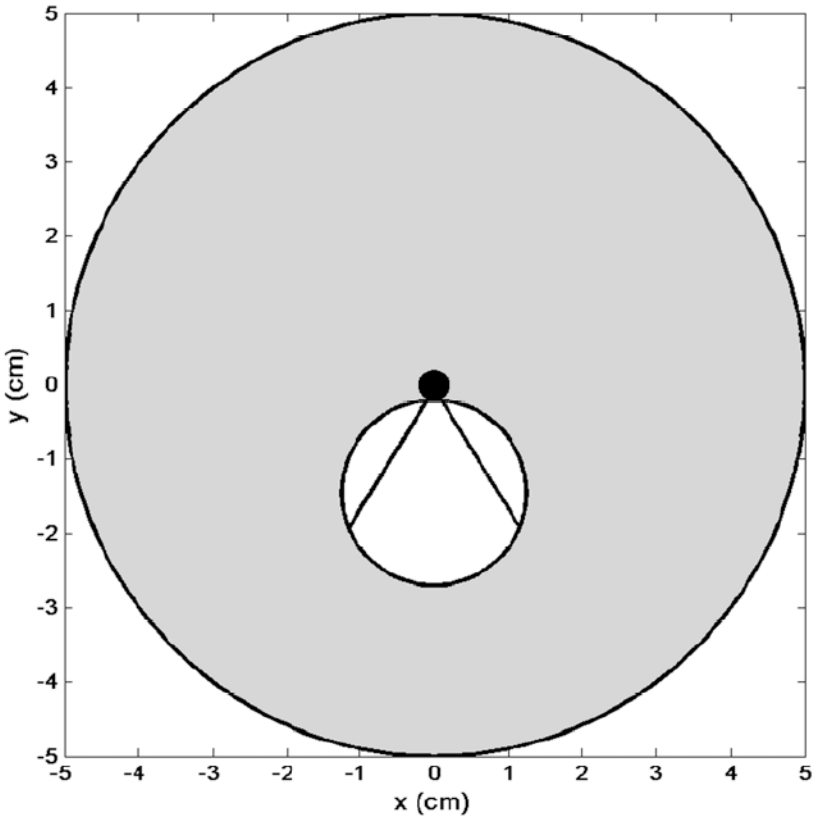

Figure 1.
Schematic of proposed dual-mode IVUS operation. Radial imaging field (gray circle) with tumor (white circle). Hyperthermia beam (straight lines indicate full beamwidth at half-maximum) from catheter (black circle) directed at tumor volume.

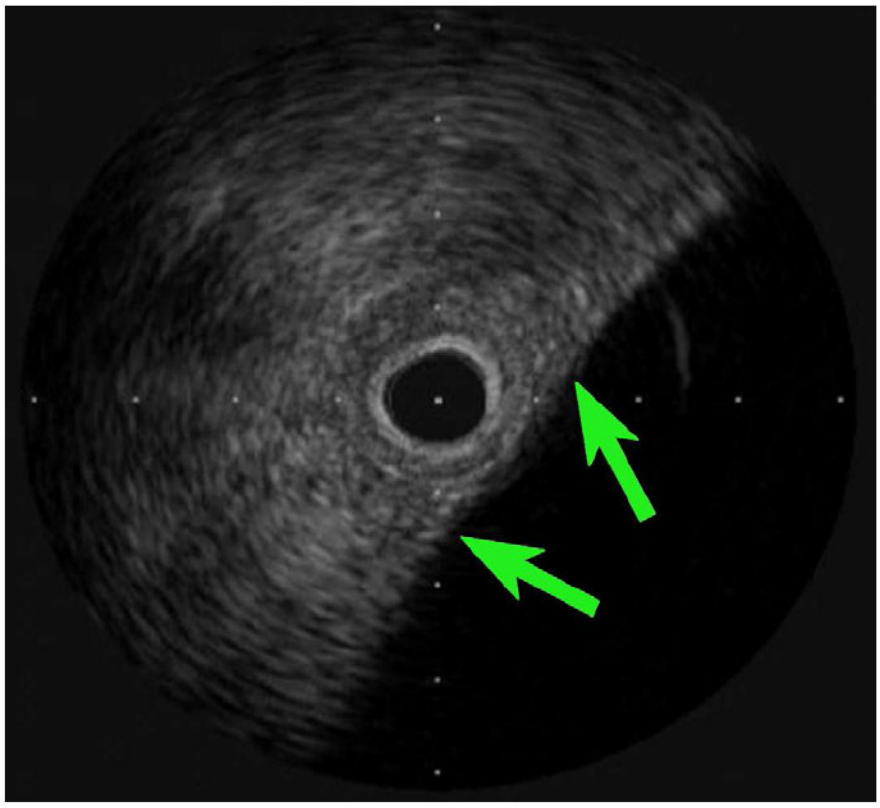

Figure 2.
40-MHz image of 2.5-cm cyst phantom, acquired with Atlantis IVUS catheter. Arrows indicate cyst wall. Tick mark spacing is 1 mm.

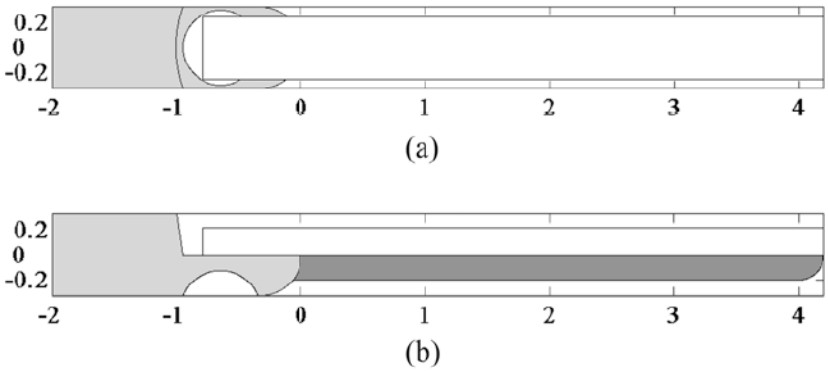

Figure 3.
Schematic of 9 MHz imaging prototype. (a) Top view of transducer bonded to metal housing (light gray). (b) Side view showing phenolic microballoon backing (dark gray). Scale in mm.

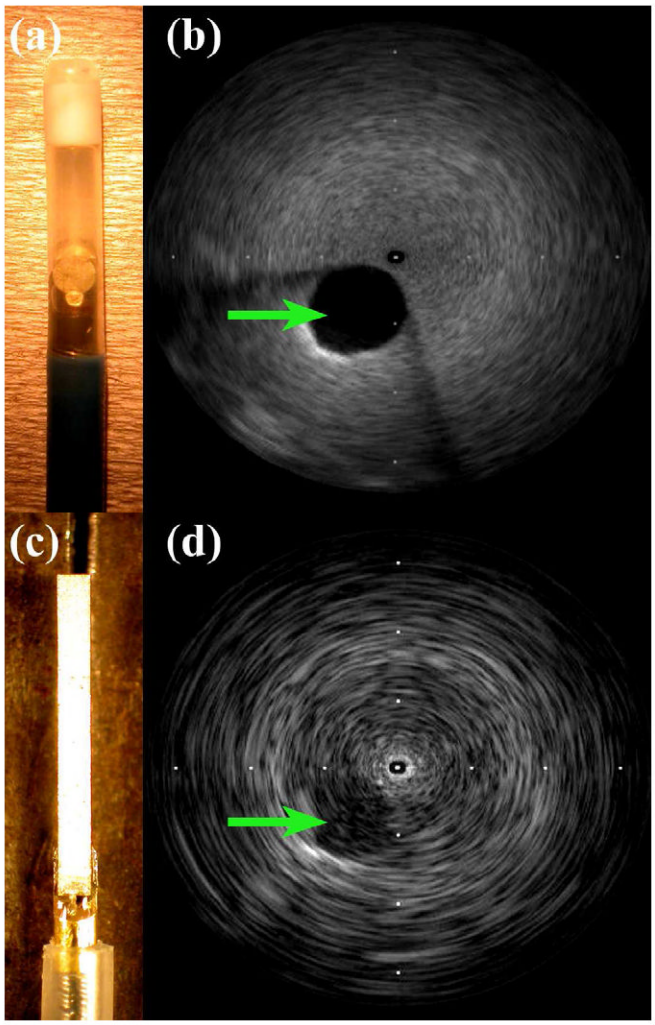

Figure 4.
Catheter devices and 9-MHz images of 2.5-cm cyst phantom. (a) 9-Fr ICE with 2.1-mm-diameter transducer. (b) ICE catheter cyst image. (c) Modified IVUS prototype outside of 3.5-Fr sheath. (d) Modified IVUS cyst image. Tick mark spacing is 16 mm.

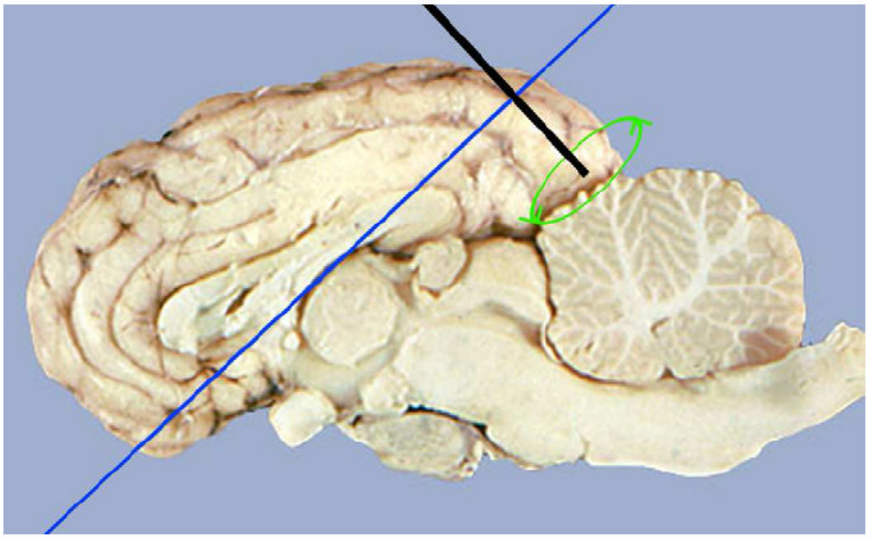

Figure 5.
Diagram of ovine brain imaging scheme. Catheter insertion (McDannold et al.) into posterior portion of superior sagittal sinus, with rotating transducer scanning a perpendicular plane (dark blue). Reproduced with permission (Miselis 2006).

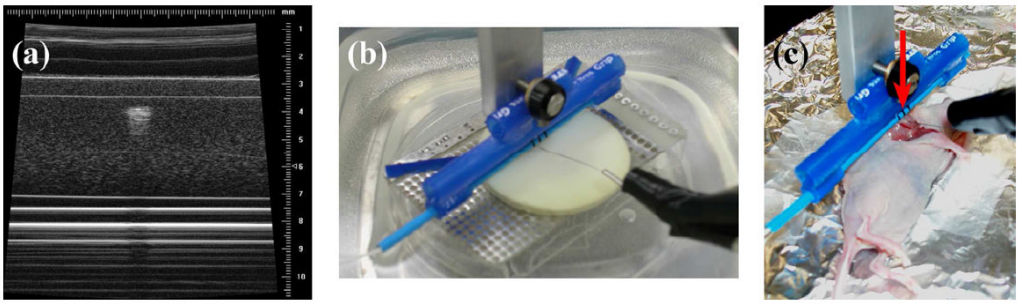

Figure 6.
Therapy experiment procedures. (a) 40-MHz VisualSonics image verifying thermocouple needle 1 mm beneath the surface in tissue-mimicking material. (b) In vitro therapy experiment setup. (c) In vivo glioblastoma therapy setup: anesthetized mouse on foil-lined heating pad. Arrow indicates transducer position.

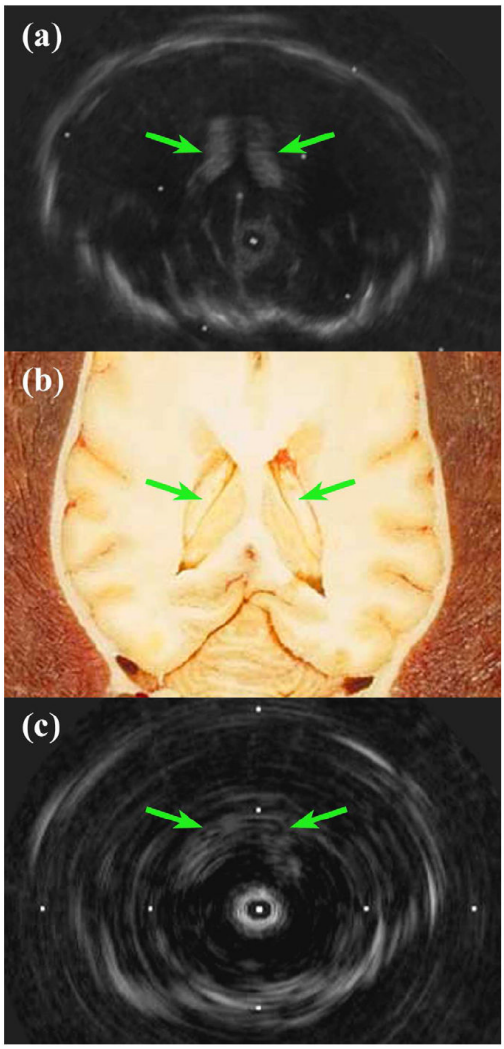

Figure 7.
Post-mortem ovine brain 9-MHz imaging comparison showing lateral ventricles. (a) 9-Fr ICE catheter image. (b) Anatomical diagram, reproduced with permission (Fletcher et al. 2006). (c) 3.5-Fr modified IVUS prototype image. Tick mark spacing is 16 mm.

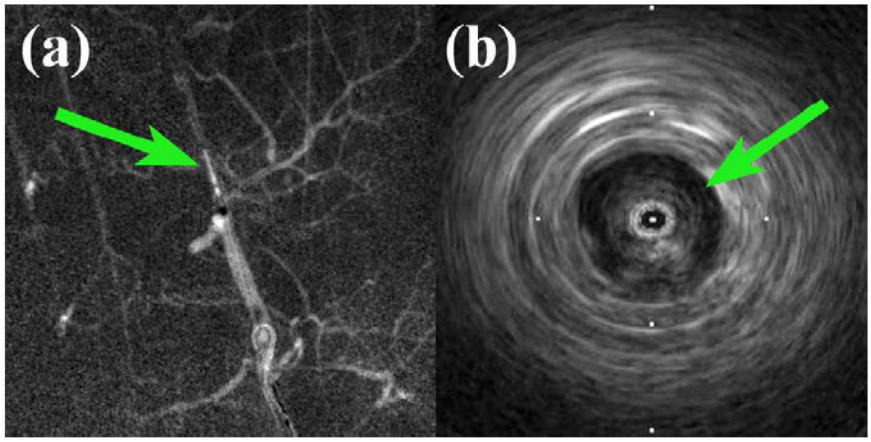

Figure 8.
In vivo porcine imaging results. (a) Angiogram showing modified IVUS prototype (arrow) in right vertebral artery. (b) 9-MHz image of vertebral artery lumen (arrow) and surrounding tissue near subclavian junction. Tick mark spacing is 16 mm.

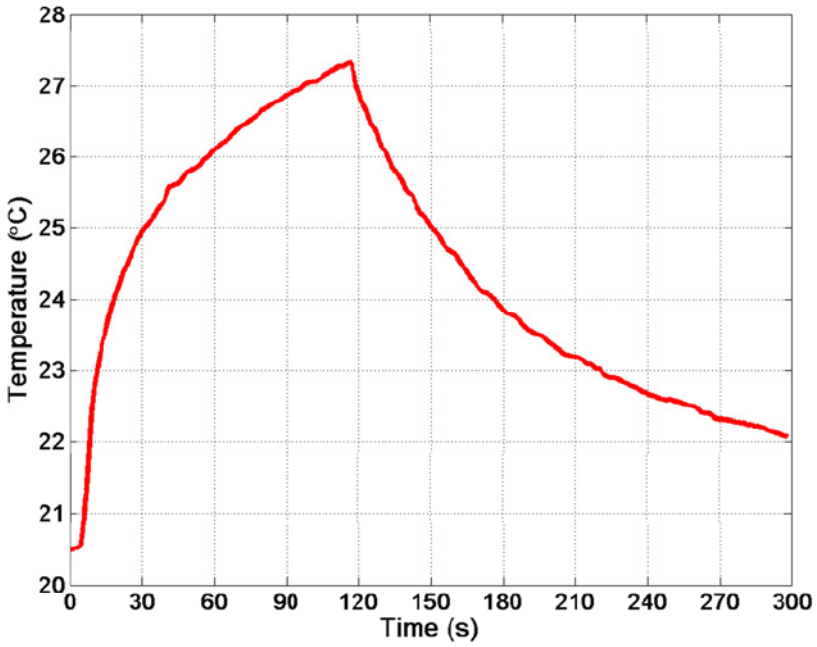

Figure 9.
Thermocouple data from in vitro therapy experiment with tissue-mimicking material. Resulting temperature rise was 6.7°C in under 2 minutes.

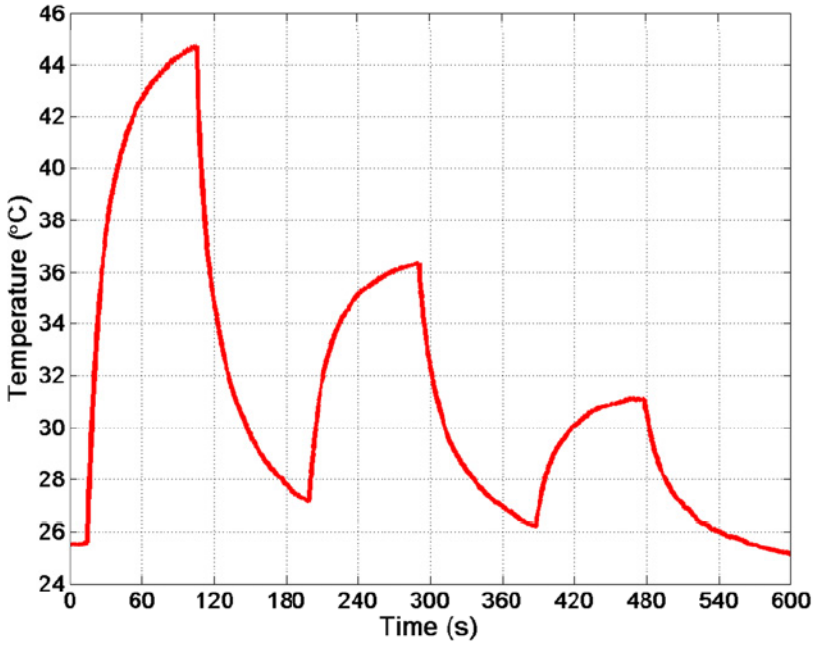

Figure 10.
Thermocouple data showing sequential temperature rises in excised glioblastoma tumor of 19.1°C, 9.2°C, and 4.9°C after 90 seconds of on-time for power levels of 700, 350, and 175 mW, respectively.

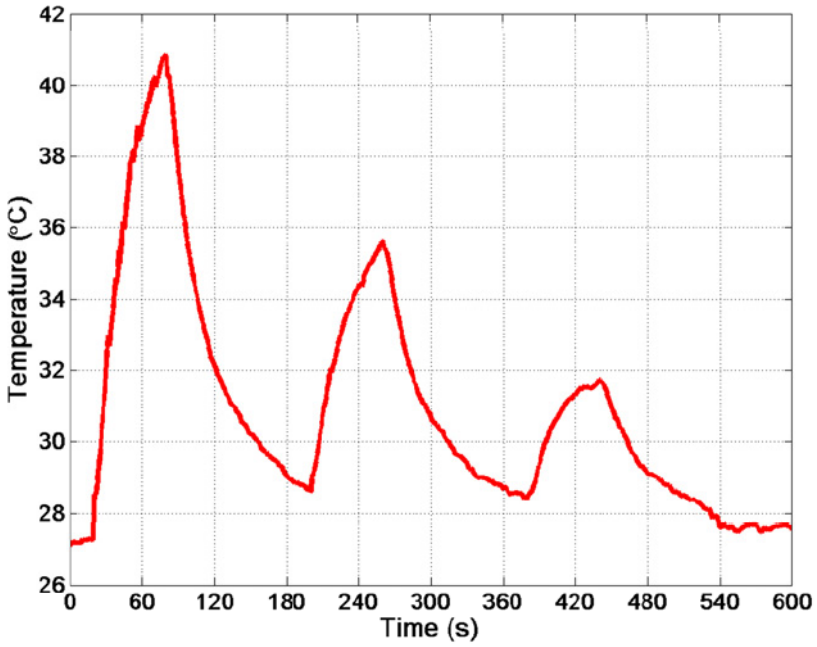

Figure 11.
Thermocouple data for in vivo xenograft glioblastoma tumor grown in the flank of a nude mouse, showing sequential temperature rises of 13.5°C, 6.8°C, and 3.0°C after 60 seconds of on-time for power levels of 700, 350, and 175 mW, respectively.

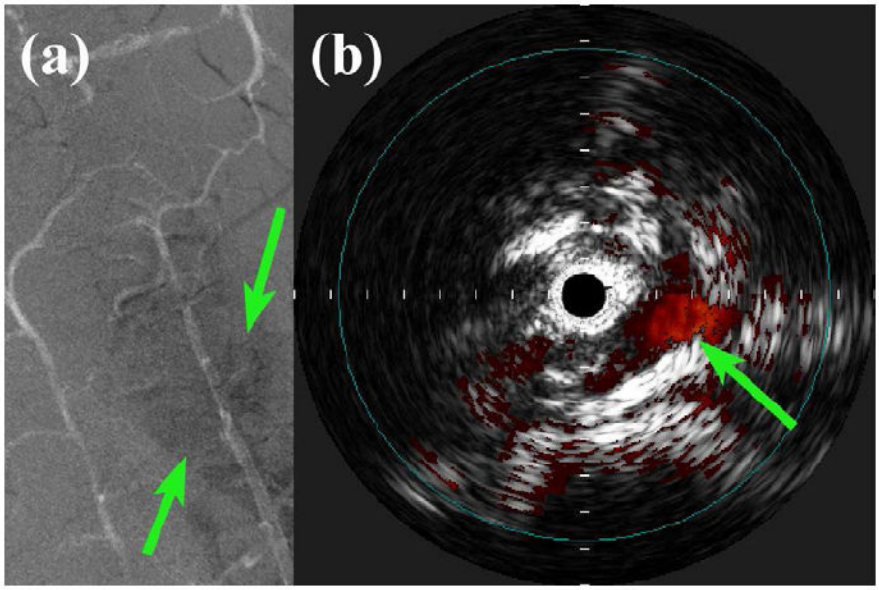

Figure 12.
In vivo porcine vascular imaging results. (a) Angiogram showing a regional hematoma (arrows) surrounding the right vertebral artery. (b) Volcano ChromoFlo image showing non-uniform flow (arrow) in the lumen near the vessel puncture site, acquired with 20-MHz Eagle Eye Gold. Tick mark spacing is 1 mm.

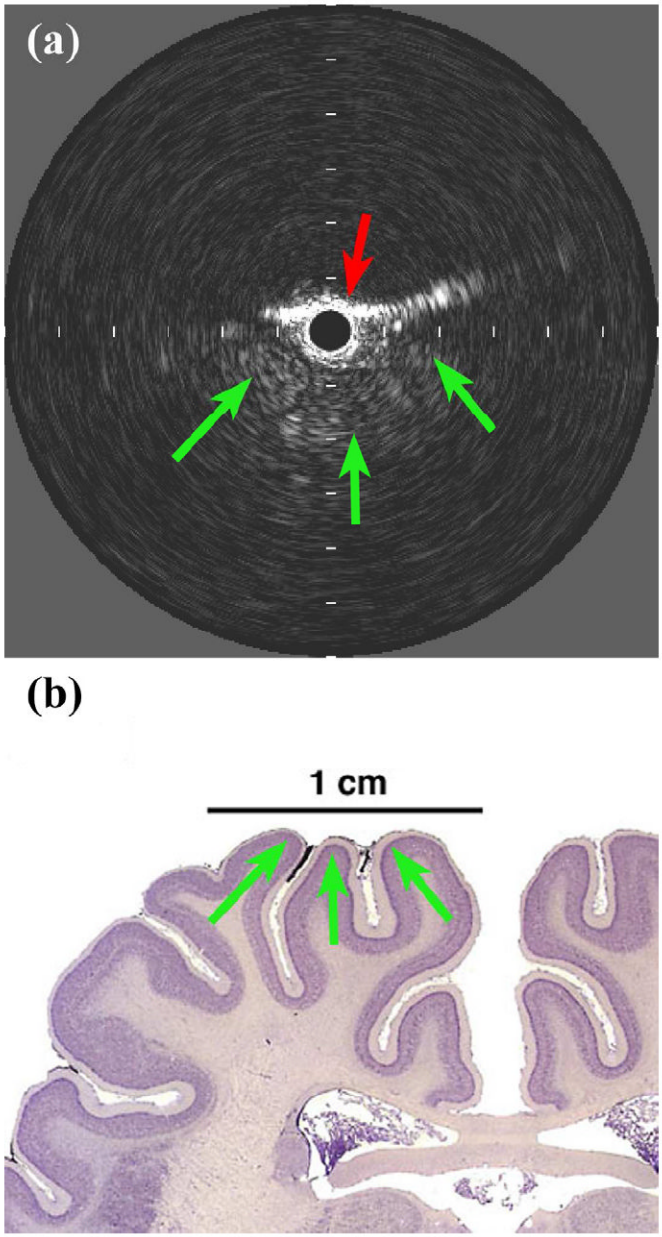

Figure 13.
In vivo porcine brain imaging results. (a) Volcano PV018 image showing bordering skull (red arrow) and three gyri in close proximity (green arrows). Tick mark spacing is 2 mm. (b) Anatomical diagram, reproduced with permission (Welker 2011).